Journal of Intelligent & Robotic Systems (2022) 105: 22
https://doi.org/10.1007/s10846-022-01631-2

SHORT PAPER

Bioinspired Legged Robot Design via Blended Physical and Virtual Impedance Control

Omid Mohseni[1] · Aida Mohammadi Nejad Rashty[1] · Andre Seyfarth[1] · Koh Hosoda[2] · Maziar Ahmad Sharbafi[1]

Received: 26 August 2021 / Accepted: 5 April 2022 / Published online: 11 May 2022

Abstract

In order to approach the performance of biological locomotion in legged robots, better integration between body design and control is required. In that respect, understanding the mechanics and control of human locomotion will help us build legged robots with comparable efficient performance. From another perspective, developing bioinspired robots can also improve our understanding of human locomotion. In this work, we create a bioinspired robot with a blended physical and virtual impedance control to configure the robot's mechatronic setup. We consider human neural control and musculoskeletal system a blueprint for a hopping robot. The hybrid electric-pneumatic actuator (EPA) presents an artificial copy of this biological system to implement the blended control. By defining efficacy as a metric that encompasses both performance and efficiency, we demonstrate that incorporating a simple force-based control besides constant pressure pneumatic artificial muscles (PAM) alone can increase the efficiency up to 21% in simulations and 7% in experiments with the 2-segmented EPA-hopper robot. Also, we show that with proper adjustment of the force-based controller and the PAMs, efficacy can be further increased to 41%. Finally, experimental results with the 3-segmented EPA-hopper robot and comparisons with human hopping confirm the extendability of the proposed methods to more complex robots.

Keywords Hybrid actuation · Bioinspired legged locomotion · Impedance control · Morphological computation

1 Introduction

Biological locomotor systems are potential blueprints for the design and control of legged robots [1] and [2]. The neuromuscular structure in biological systems conveys the idea that body mechanics and neural control are inextricably linked together. The human body comprises hundreds of muscle-tendon complexes (MTC); a high-performance unit with a neuromechanical control system. The impedance formulated in the force-length and force-velocity relationships [3] governing these MTCs can be varied by changes in physical properties of the muscle (e.g., muscle thickness, tendon stiffness) or be tuned by the activation signals coming from the central nervous system [4]. This neuromuscular system leverages the biological actuators by physically or virtually adapting their impedance.

Inspired by the functional performance and neuromechanical control of biological muscles [5], appropriate design of the physical body dynamics and the controller can largely enhance the locomotion performance [6]. By adding compliance to the body of a given robot or adapting the existing compliant elements in the body, part of the locomotion control problem can be shifted from the brain to body dynamics [7] and [8]. The use of the body as a computational resource in conjunction with the brain is a concept generally known as control embodiment [9]. The control embodiment is quite advantageous in reducing the control effort [10], minimizing energy consumption, protecting

✉ Omid Mohseni
omid.mohseni@tu-darmstadt.de

Aida Mohammadi Nejad Rashty
aidamnr@sport.tu-darmstadt.de

Andre Seyfarth
seyfarth@sport.tu-darmstadt.de

Koh Hosoda
hosoda@sys.es.osaka-u.ac.jp

Maziar Ahmad Sharbafi
sharbafi@sport.tu-darmstadt.de

1 Lauflabor Locomotion Laboratory, Centre for Cognitive Science, TU Darmstadt, Darmstadt, Germany

2 Graduate School of Engineering, Osaka University, Toyonaka, Japan

motors from impacts, decreasing peak motor power requirements, and reducing the amount of required sensor data [11–13]. Compliant elements come in different forms with fixed or variable stiffness and have different configurations, mainly categorized as: series elastic actuators (SEAs) [1] and [14], parallel elastic actuators (PEAs) [15–18], and in combination (SPEAs) [19] and [20]. Numerous studies have already applied such combinations for improving the efficiency or robustness of legged robot locomotion [10–12, 21, 22]. The search for the best arrangement among these actuators showed that for each specific task, one could be preferred over the others [23] and [24]; meaning that there is still no winning design. Moreover, adaptable compliance as found in biological systems provide further significant advantages over traditional actuation for legged robots [6, 14, 25, 26]. However, despite the significant progress in the development of variable impedance actuators (VIA) in recent years, they are not still comparable with their biological counterparts regarding efficient performance in a wide range of tasks and motion conditions [27].

As an alternative to the aforementioned elastic actuators, in [28], we suggested combining pneumatic artificial muscles (PAM) and electric motors (EM) in the EPA (electric-pneumatic actuator). This novel hybrid actuator can provide direct access for virtual and physical impedance adjustment in robots. On one hand, PAMs are the closest actuators to biological muscles [29] and [30] and they can be considered as cheap and reconfigurable [31] physical impedance. Because of their high power to weight ratio, this adjustable physical impedance is advantageous for periodic movements such as legged locomotion [32]. On the other hand, EMs are suitable actuators for precise control and implementing virtual impedance control. Different arrangements (SEA, PEA, SPEA) and even implementation of multi-articular coupling using PAMs provide the required flexibility of EPA for benefiting from morphological computation and control embodiment. Within this hybrid design, different features of legged locomotion can be optimized; e.g., the addition of parallel PAMs to EMs can make the system more efficient (compared to EM) and more robust against impacts [16] and [33].

In this work, we develop two EPA-based robots, namely EPA-Hopper-I & -II, based on the blended physical and virtual impedance control concept. In the knee joint of these robots, the PAM pressure tunes the physical impedance while the EM controls the virtual knee impedance. Inspired by human motor control [34] and [35], the leg force (equivalently the ground reaction force (GRF)) can be a helpful feedback signal to tune the muscle activation and consequently the virtual impedance. With this insight, we previously developed force modulated compliance (FMC) control methods to adjust the stiffness (impedance) of hip and ankle to control a variety of gaits [36, 37]. More recently, we utilized the FMC on the knee joint of the 1D MARCO-Hopper II robot and showed that this controller could generate stable hopping patterns [38]. Similar to the virtual model control framework [39] and [40], here, we consider a virtual knee spring in which the GRF modulates the stiffness. The simple design and the ability of this control method to be extended to other robots (e.g., with more degrees of freedom) are the key features of FMC control that are investigated in this study. The contribution of this paper is threefold: 1) verifying the applicability of a bioinspired GRF-based control (FMC) on a simple segmented hopper robot and its extendability to an anthropomorphic hopper robot, 2) investigating the benefits of tuning physical and virtual impedance in terms of efficiency and performance, and 3) introducing a modified version of the FMC controller and harnessing the potentials of PAMs to achieve higher efficiency, performance, and human-like motion behavior. In the following, we describe how the blended impedance control is developed and applied to the EPA-hopper robots, analyze the effects of the virtual and physical impedance on efficiency and performance, and finally compare the outcomes with human hopping.

2 Methods

The first part of our blended control scheme is the physical impedance control addressed in the following by the EPA actuation system. Then, we explain the second part by introducing the force modulated compliant knee (FMCK) as the bioinspired virtual impedance control approach. We also present a measure for evaluating the performance and efficiency of the controlled movement, followed by human hopping experiments to be considered as a reference model.

2.1 Physical Compliance Control with EPA

Here, we introduce the EPA actuation concept as a platform for simple adjustment of the physical compliance using the PAMs. We present the models and the hardware setups of the developed EPA-based hopping robots, *EPA-Hopper-I* and *EPA-Hopper-II*, which respectively have a 2-segmented and 3-segmented leg design. This methodology can be extended for more complex robots in the future.

2.1.1 Hybrid Actuation in EPA

The collaboration of EM and PAM offers a hybrid variable impedance actuation that can mimic biological actuation. Having PAMs in series with an EM gives the system the ability to absorb shocks and tolerate impacts which is beneficial for human-robot interactions. Moreover, this serial configuration can contribute to increased energy efficiency

in cyclic tasks. PAMs can also be installed in a parallel configuration with the EM to reduce power or torque requirements, provided that they are appropriately tuned. A PAM can cross two joints of an articulated robot in another possible arrangement, acting as an energy exchanger. The biarticular arrangement is advantageous for increasing energy efficiency [41] and simplifying control task [14]. In Fig. 1, a general schematic of these arrangements is depicted for a three-segmented mechanism (e.g., a two-segmented leg and a trunk). A specific combination of the three arrangements (shown with different colors) can provide an optimal solution for different applications. Each PAM can be used as an adjustable compliant element or an individual actuator. This hybrid actuation system can be applied to any legged robot.

In the following, we first describe the design of EPA-Hopper-I and then its extension to the 3-segmented leg in EPA-Hopper-II.

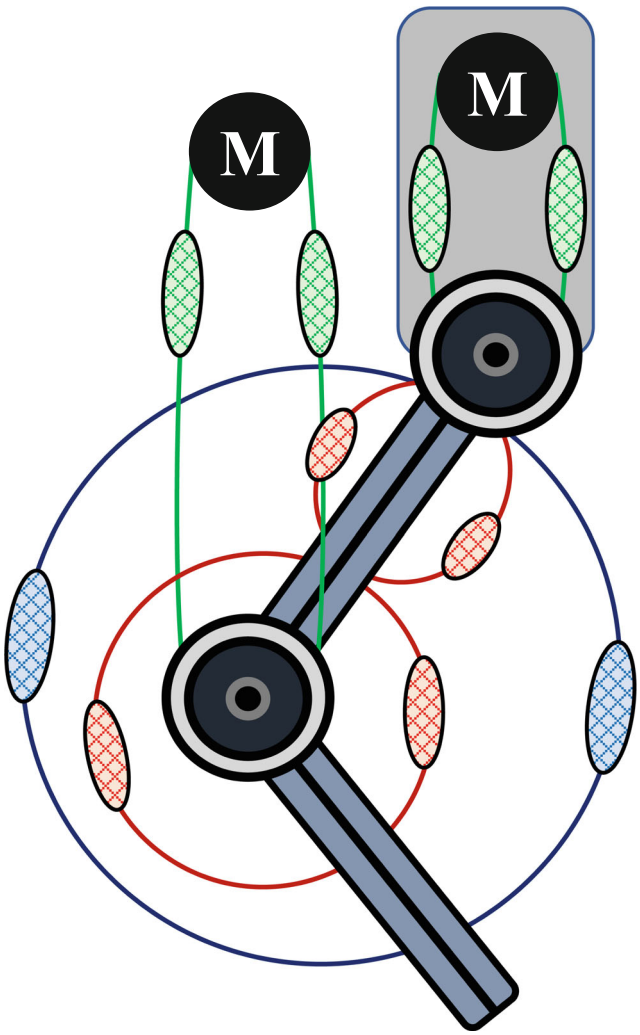

Fig. 1 General schematic of Electric-Pneumatic Actuation showing different possible arrangements of electric motors (M) and PAM in a three segmented mechanism. Here, the green, red and blue colors represent series, mono-articular and bi-articular PAMs, respectively

2.1.2 EPA-Hopper-I

To concentrate on the blended impedance control concept, we only select two mono-articular PAMs (knee extensor and a flexor) from the general arrangement shown in Fig. 1. These two McKibben PAMs are placed in a parallel configuration and act antagonistically on the knee joint; see Fig. 2a. This robotic leg comprises two actuated degrees of freedom (DoF) moving in 2D, with the hip joint constrained to move only in the vertical direction to exclude the body posture control. Figures 2b and 2c show the robot and its detailed simulation model.

The thigh and shank segments of the leg are made of hollow lightweight carbon fiber tubes to keep the weight and moment of inertia low. Most other mechanical parts, except the bearings, are 3D printed with PLA and ABS thermoplastics. In this setup, the leg is equipped with two electric motors and two hand-made PAMs. The two brushless direct current (BLDC) motors (HYmotor E8318-120kV) are located at the hip co-axially to minimize the leg moment of inertia. The first one actuates the hip joint directly, and the other one drives the knee joint via a rope-pulley transmission with a moment arm ratio of 1:5. Using a rope and pulley system instead of a gearbox helps avoid friction and high mechanical stiffness in the transmission chain. Therefore, the direct drive for the hip actuation and the quasi direct drive for the knee ensures the transparency between the motor and the environment [42]. This setup facilitates torque control implementation using motor current sensing. The electrical motors are also equipped with current sensors and AMT10-series incremental encoders for position measurements. Each PAM on the robot operates with two continuous valves (PVQ-series proportional solenoid valves) for supplying and exhausting the air. The air pressure is provided from a JUN-AIR (Quiet Air 6-15) compressor. We used PSE530 sensors to control the PAM pressure.

2.1.3 EPA-Hopper-II

To develop EPA-Hopper-II (Fig. 2d), we extended EPA-Hopper-I by addition of a 3D printed foot as well as an ankle extensor PAM and an ankle flexor spring, mimicking Soleus (SOL) and Tibialis Anterior (TA) muscles, respectively. As the ankle joint in humans has shown to have a more elastic behavior than the knee and hip [43], no electrical motors were considered for this joint in this setup, and as a result, it is passively actuated by the SOL PAM and TA spring. The compliant curved foot is designed to resemble the shape of the human foot. A rubber sheet is also attached beneath the foot to absorb the shock during initial ground contact further. The SOL-like PAM is located between the heel and top of the shank to support the ankle extension passively.

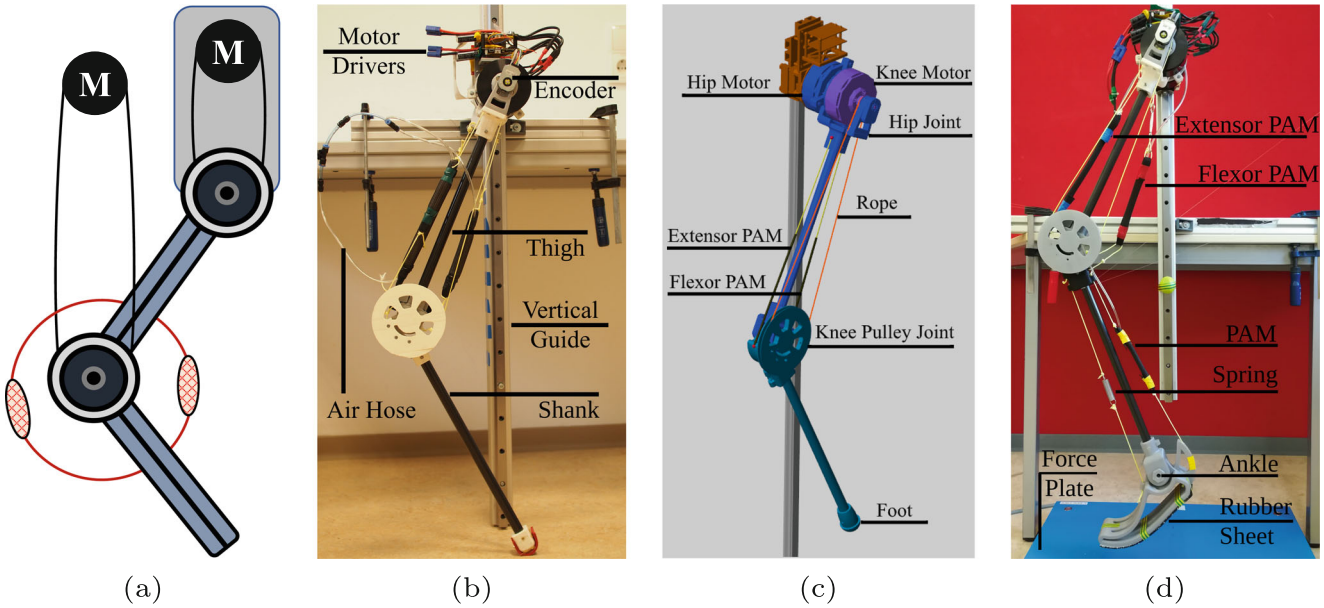

Fig. 2 Robotic setups. (a) a schematic drawing of EPA-Hopper-I with two-segmented leg, two motors for hip and knee joints and two antagonistic PAMs at the knee joint, (b) EPA-Hopper-I robot, (c) the simulation model of EPA-Hopper-I, developed in MATLAB SimMechanics and (d) the EPA-Hopper-II, an extension of EPA-Hopper-I with an additional 3D-printed foot, ankle extensor PAM and ankle flexor spring

In both setups, a lithium polymer battery provides the power source, which can deliver high peak current to the motor drivers. For measuring GRF during hopping, a force plate is placed under the leg. The kinematics are measured using three motion capture cameras. Finally, with xPC Target of MATLAB, we control the robot using Simulink in real-time and collect data at the rate of 1 kHz.

To ensure safety while conducting experiments with the robot, multiple safety measures are implemented in the xPC Target of Matlab. The desired motor currents for both hip and knee are saturated to a maximum of 50 A. The knee and hip angles are also limited to a range that results in a reasonable motion output. On top of these measures, to further ensure that the safety conditions are fulfilled, a kill switch is implemented to shut off the electronics manually.

2.1.4 Simulation Model

To develop simulation models of EPA-Hopper robots that best matches the experimental setup, we imported the 3D CAD-designed parts of the leg along with their inertia properties directly into the SimMechanics environment of MATLAB. Moreover, by means of a 1-DoF prismatic joint as a guide, we limited the leg motion to the vertical direction; see Fig. 2c. For modeling the ground and contact forces, we utilized the Simscape Multibody Contact Forces Library with friction and nonlinear force law. The parameters related to the simulated ground (e.g., stiffness, damping, and maximum penetration for full damping) and also the friction values of the joints were all assessed by conducting several experiments further to match the leg model with the robot in practice. Table 1 summarizes the parameters considered for the simulation model of EPA hopper robots.

To incorporate the PAMs into the simulations, we modeled them as prismatic actuators acting antagonistically on the knee joint. The output forces generated by these actuators are predicted based on a dynamical muscle-like model, which was shown in our previous work to have an acceptable precision in predicting the actual PAMs' dynamic behaviors [29]. Our biological model of PAM consists of a contractile element in parallel with a compliant component as:

$$F_{PAM}(P, l, v) = PFf_{la}(l)f_v(v) + Ff_{lp}(l), \quad (1)$$

where P is the instantaneous pressure inside the PAM, playing the role of muscle activation, and F is a constant corresponding to the maximum isometric force in the Hill-type muscle model. The two polynomial functions f_{la} and f_{lp} describe the dependency of PAM force to its length l, representing the force-length pattern of biological muscles. Finally, f_v is a linear function of velocity v, defined as the rate of PAM length variations. For more details regarding the PAM modeling and identification, please refer to [29]. In the EPA-Hopper-I simulation model, we considered a pair of mono-articular PAMs, one extensor and one flexor, placed on the knee joint with lengths of 22 cm and 16 cm, respectively. The parameters related to model these PAMs were identified in separate experiments as explained in [29].

Table 1 Identified physical parameters of EPA, used in the simulation model

Parameter	Definition	Value (units)
l_s	Shank length	0.46 (m)
l_t	Thigh length	0.42 (m)
r_1	Driver pulley diameter	0.02 (m)
r_2	Follower pulley diameter	0.10 (m)
h_{td}	Hip height at touchdown	0.78 (m)
m_s	Shank mass	0.265 (kg)
m_t	Thigh mass	0.974 (kg)
m_h	Hip mass	0.806 (kg)
m_r	Knee motor mass	0.728 (kg)
m_a	Ankle mass	0.101 (kg)
m_f	Foot mass	0.160 (kg)
d_g	Guide damping	0.0268 (N/(m/s))
f_g	Guide friction force	1.7611 (N)
k_{gc}	Ground contact stiffness	54217.67 (N/m)
d_{gc}	Ground contact damping	248.839 (Ns/m)
l_{gc}	Ground penetration	$4.3835e-3$ (m)
τ_m	Motor maximum torque	4 (Nm)
ω_m	Motor maximum speed	2600 (rpm)
k_τ	Motor torque constant	0.08 (Nm/A)
g	Gravitational acceleration	9.81 ($m.s^{-2}$)

2.2 Virtual Compliance Control with FMCK

Achieving a stable bouncing pattern or hopping in place while experiencing consecutive ground impacts and other possible disturbances is a challenging problem [10]. It was shown that by injecting a predetermined amount of energy greater than the system losses during a hopping cycle, an actuated prismatic leg (MARCO-Hopper) could generate stable hopping [44]. Even with a simple feed-forward control with minimal sensory information, stable hopping with a segmented leg having sufficient robustness against moderate perturbations is achievable [45]. However, it requires a precise set of parameters to function, which makes it in turn sensitive to changes, uncertainties, and large disturbances. On the other hand, feedback controllers overcome these drawbacks by incorporating some additional sensory information. Among feedback control methods, the virtual model control (VMC) [39] is an exemplary approach for robust hopping motion with a tunable hopping height, just by emulating a virtual spring for mimicking human leg behavior in hopping [40]. Faster recovery from ground-level perturbations counts as one advantage of VMC in comparison to feed-forward approaches.

In a biomechanical study, Geyer et al. attempted to mimic the human reflex system, where muscle length, velocity, or force were used for proprioceptive feedback [46]. They showed that positive force and length feedback of an extensor muscle on a two-segmented leg model could result in periodic hopping [46], while force feedback has further advantages regarding improved performance and reproducing human-like elastic leg behavior. Later, this positive force feedback was further analyzed with respect to muscle properties [47] and the sensor-motor-map concept [48]. Recently, in [49] the applicability of the neuromuscular reflex controller was tested in both single- and two-leg robots. The combination of feed-forward and feedback signals for hopping control was also investigated in [50]. It was found that this combination improves hopping stability and recovery from perturbations, thanks to the nonlinear Hill-type representation of intrinsic muscle properties. However, the performance of these methods relies on the level of details considered for implementing the controller (i.e., the nonlinear force-length-velocity relationship). Moreover, finding the right parameters of these controllers and their tuning demands an exhaustive search [46–48, 51].

Inspired by the positive force feedback concept [46], here we introduce the force modulated compliant knee (FMCK) method to control the EPA robots. Similar to our previous *FMCH* [36] and *FMCA* [52] control methods that respectively tune hip and ankle compliance, here, we use the ground reaction force (GRF) to modulate the knee compliance. In the FMCK control method, the knee torque τ_k is given by an adjustable spring equation:

$$\tau_k = C \times GRF \times (\phi_k - \phi_{k0}) \tag{2}$$

where GRF, ϕ_k, ϕ_{k0} and C are the ground reaction force, the current knee angle with respect to the thigh, the nominal knee joint angle, and the normalized stiffness, respectively. Hence, the FMCK can be interpreted as a simplified reflex control in which the muscle and muscle force are replaced by a spring and the leg force (measured by GRF), respectively.

To implement the controller, the hopping sequence is divided into flight and stance sub-phases with detection of the foot collision in-between using the measured GRF signal. During the flight phase, knee and hip joints are position controlled to predefined target angles using independent PD controllers. The parameters of the PD controllers are manually tuned to reach the desired leg posture before the foot touches the ground and thus ensure repeatability of each experiment. At the onset of foot collision, a PD transition controller from flight to stance phase is employed for both hip and knee motors for a short period ($t_c = 5$ ms). This collision phase controller has a relatively low P gain but a high D value to absorb the impact energy during the

collision and prevent undesired oscillations after landing. After this short period, the controller switches to FMCK for controlling the knee joint in the stance sub-phase, and the hip motor is set free. The knee motor desired current (computed from Equation 2) is inputted into the motor driver, where the low-level field oriented control (FOC) runs at a rate of 20 kHz. Figure 3 shows the block diagram of this control approach.

2.3 Comparison Metrics

To evaluate and compare the results in the following sections, we define three metrics, namely *hopping height*, *energy consumption*, and *efficacy*, all measured once the robot performs stable hopping. The *hopping height*, denoted by h hereinafter, is defined as the difference between the maximum hip height and a predetermined hip height at touchdown:

$$h = h_{max} - h_{td} \tag{3}$$

The *energy consumption* E is calculated as the summation of knee and hip absolute work during both stance and flight phases, as follows:

$$E = \int_T |\tau_k \dot{\phi}_k| dt + \int_T |\tau_h \dot{\phi}_h| dt \tag{4}$$

where τ_k and $\dot{\phi}_k$ indicate the knee torque and velocity, respectively. τ_h and $\dot{\phi}_h$ are defined similarly but for the hip joint, and T is the period of hopping cycle. To define the efficacy criterion, we use the ratio between the required energy for reaching a certain hopping height and the consumed energy in the robot. During the stance phase, the robot needs to absorb the kinetic energy at touchdown and generate the same amount while moving in the opposite direction at the take-off moment to return to its initial starting state. Therefore, two times the kinetic energy at touchdown could be a measure for normalizing the robot mechanical work (E) and defining the efficacy. An easy way to find the kinetic energy at touchdown is calculating the potential energy difference over the hopping height h as mgh where m is the total mass of the robot and g is the gravitational acceleration. As a result, the *efficacy* ρ is computed as:

$$\rho = \frac{2mgh}{E} \tag{5}$$

With this definition, the larger the efficacy, the higher the cost-effective movement.

2.4 Human Hopping Experiment

The hopping experiments were conducted with seven young healthy subjects; 6 males and 1 female, age: 24.14 ± 3.33 years, mass: 68.5 ± 9.7 kg. All participants provided written informed consent. The subjects were instructed to perform vertical hopping on both legs with their hands resting on their hips. For the first hopping trial, subjects were asked to hop with their preferred hopping frequency (PHF) for 20 sec. The purpose of this trial was to calculate the PHF of each individual numerically. After that, they were cued with a signal tone by a metronome and were asked to hop with 75 %, 100 %, 125 % and 150 % of their PHF. Subjects repeated hopping in each frequency six times, lasting 35 sec each, with two minutes rest in between. Each trial started with 5 sec of preparation, followed by 5 sec of standing still on force plates, then 20 sec of continuous hopping, and finally 5 sec of standing still again.

For kinematic data collection, 10 motion capture cameras (Qualisys Type 5+/6+, 500 Hz) were employed to record the movements of 21 markers placed on anatomical locations with minimal skin/muscle motion. Moreover, for measuring the ground reaction force (GRF) during hopping, two piezoelectric Kistler force plates (Type 9260AA) were used for the left and right leg individually. Finally, OpenSim

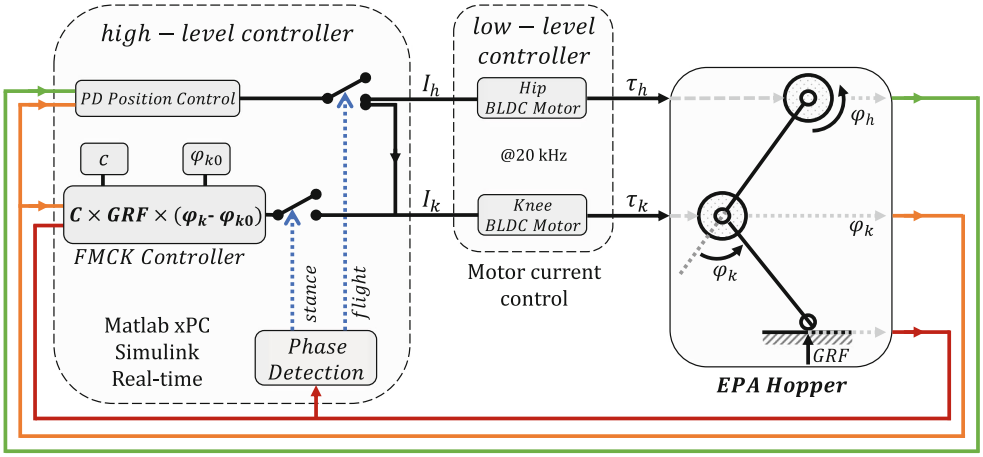

Fig. 3 Schematic overview of the control system architecture that uses ground reaction force (GRF) and joint angles (ϕ_i) as feedback signals for control of hopping. The high-level controller is implemented in real-time with MATLAB Simulink xPC target. The interface between xPC target machine and other parts is through an EtherCAT communication bus at 1 kHz

[53] along with its inverse kinematics and inverse dynamics tools, were used to calculate the hip, knee, and ankle angles as well as the corresponding joint torques.

3 Results

We conducted the EPA simulations/experiments in three different scenarios. In scenario A, we put the FMCK controller to test by relying only on the electrical motors (i.e., with PAMs being turned off). The purpose of this scenario is to evaluate the performance of our proposed virtual impedance controller in achieving stable hopping. In scenario B, we incorporated the PAMs into the hopping control while inflating with a fixed amount of air pressure. Then, in scenario C, we added another degree of freedom to the leg by adding a passive foot and compared the results with human data in hopping.

In all of the following simulations/experiments, the PD values for the hip and knee joints in the flight phase are chosen as $[P = 5, D = 0.2]$ and $[P = 2, D = 0.04]$, respectively. Moreover, the maximum output torque of the knee and hip motors in simulations is set to $\tau_m = 4\,\text{Nm}$ to match the values of electrical motors on the experimental setup.

3.1 Virtual compliance control with FMCK

The adjustable virtual compliance is determined with the normalized stiffness C and the rest angle ϕ_{k0} (in Equation 2). To assess the performance of our proposed FMCK controller, we first searched for the values with which the robot can hop stably. Note that in this scenario, the PAMs were off completely. Here, stable periodic hoppings of the robot were checked and confirmed by the return maps of the apex height. The hopping heights achieved in terms of the values of the FMCK control parameters are shown in Fig. 4a. For illustration purposes and better comparison Fig. 4b displays a zoomed area of the former figure in 2D. According to this figure, it can be seen that (1) various hopping heights up to 25 cm can be achieved with the FMCK controller, (2) hopping with different heights can be regulated, especially by tuning ϕ_{k0} in the range of $0^\circ \leq \phi_{k0} < 50^\circ$, and (3) there is a range of control parameters ($[C, \phi_{k0}]$ values) to reach a certain hopping height. Thus, the control parameters can be used to optimize other metrics such as energy efficiency. This property can be analyzed by Figs. 4c and 4d which illustrate the consumed energy of the robot for the same range of control parameters. These two graphs make it possible to find an efficient solution for a specific desired hopping height. For example, by setting C to 0.3 m/rad, hopping height of 25 cm can be achieved with $0^\circ \leq \phi_{k0} \leq 12^\circ$ while increasing the rest angle could reduce the consumed energy from 50 J to 42 J. This 16% energy consumption reduction is obtained by tuning one control parameter without disturbing the hopping performance.

We implemented the same virtual compliance control approach (described in Fig. 3) on the EPA-Hopper-I (and -II) robot to validate the simulation model and test the performance of the controller in practice. Since the objective is to test the FMCK (virtual impedance) control quality without additional physical impedance, both flexor and extensor PAMs were turned off during hopping; see Extension 1 for the robot hopping performance in this case.

To compare the simulation and experimental results, Fig. 5 (first row) demonstrates the hip position, GRF, and consumed power in one hopping cycle. Here, the control parameters are set to $C = 0.07\,\text{m/rad}$ and $\phi_{k0} = 0$ for both simulation and experimental trials. As seen in Fig. 5a, the hip position follows a periodic sinusoidal pattern with a frequency of $f = 1.53\,\text{Hz}$. The simulation can reproduce the hip position observed in the experiment as a measure for kinematic behavior. Figure 5b and 5c show that the pattern and magnitude of the GRF and power profiles of the knee and hip joints resemble those of simulations and are commensurate with them. Contrary to the simulation outcomes, the GRF (and consequently the power) is jittery in the experiments. This discrepancy might come from the imprecise contact model. However, the experiments and simulations' general kinematic and energetic behavior are matching.

Calculation of the metrics for this experiment shows a hopping height of $h = 17.9\,\text{cm}$, energy consumption of $E = 40.59\,\text{J}$ and efficacy of $\rho = 24.85$. Regardless of the stable hopping motion obtained in using this controller, the efficacy can be further improved by using the EPA design, which is described in the following.

3.2 Physical compliance control with EPA

In this scenario (B), tuning the physical compliance by setting an appropriate PAM pressure could complement the virtual compliance control (FMCK). To investigate the influence of the PAMs on the hopping performance and efficiency, we chose the same control parameters for both simulation and experiment as scenario A. After searching for appropriate PAMs' compliance, we set the initial air pressure inside the extensor and flexor PAMs to $P = 0.6\,\text{MPa}$ and $P = 0\,\text{MPa}$, respectively. The results of this scenario are shown in Fig. 5 (second row). The first observation from Fig. 5d is the increased hopping height $h = 19.16\,\text{cm}$ compared to Scenario A (Fig. 5a). This improvement is achieved with less energy expenditure than in the previous scenario ($E = 39.68\,\text{J}$) according to Fig. 5f. Computing the efficacy metric in this case yields $\rho = 26.62$ which shows an improvement of 7.1% compared to that of

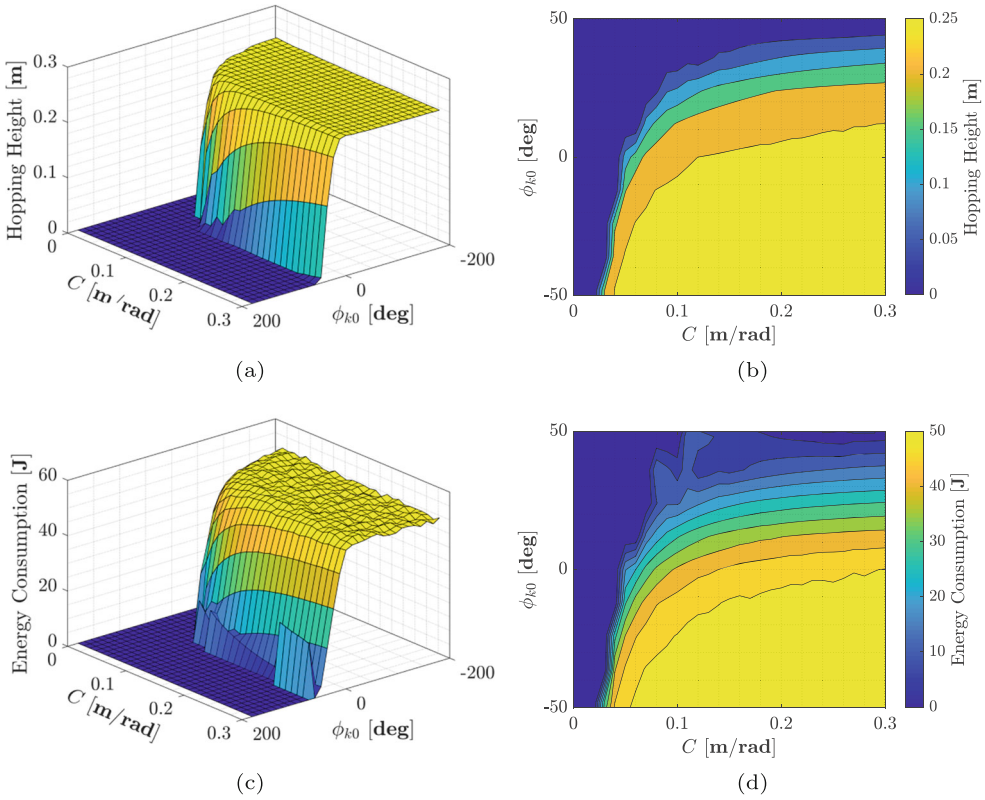

Fig. 4 Performance of FMCK controller in terms of hopping height and energy consumption; (a) achievable hopping height h by the FMCK controller for different values of gain and offset. $[C\ ,\ \phi_{k0}]$ pair values pertaining to zero hopping heights in this figure denote either unstable or aperiodic hops, (b) zoomed contour of the hopping height, (c) energy consumption for different controller parameters, and (d) 2D illustration of the energy consumption. Similar to (a,b), zero energy values in (c,d) figures correspond to failed hopping

scenario A. The overall GRF pattern (Fig. 5e) is also more human-like (curved, instead of plateau) than that of scenario A (Fig. 5b). This result shows that the addition of PAM to the robot can support the motors to consume less energy and help improve the overall performance.

3.3 Extended Applicability of Blended Impedance Control

To support the comparison of the robot's kinematic and dynamic hopping behaviors with those of humans, we applied the blended impedance controller to the three-segmented EPA-Hopper-II robot. This robot includes the foot to resemble better the morphology of the human leg. We kept the same control system of the EPA-Hopper-I. The ankle joint is controlled passively by an ankle extensor PAM (mimicking SOL muscle) and a metal spring (representing TA muscle) as shown in Fig. 2a. Interestingly, the same FMCK control parameters used for EPA-Hopper-I ($C = 0.07$ m/rad and $\phi_{k0} = 0$) can stabilize EPA-Hopper-II when the SOL PAM is pressurized at least with $P = 0.3$ MPa. The results obtained from this experiment are depicted in Fig. 6. Stable hopping is achieved despite the addition of a third DoF, which changes both the kinematics and the leg's dynamical behavior. This outcome supports the extensibility of the proposed bioinspired control concept to more complex robots with minimum required changes. The next achievement is the similarity between the robot and human hopping behavior, shown in Fig. 6 (Extension 2). As hypothesized, the addition of the foot improves the similarity to human hopping. Figure 6b demonstrates that the GRF pattern of EPA-Hopper-II looks more like the single peak pattern observed in the human hopping. In Fig. 6c, we normalized the consumed power to the body weight (BW) and then by considering the hopping height ratio. For this, we calculated the normalized hopping height for human (α_h) and robot (α_r) as the ratio of the hopping height to the leg length. For a fair comparison, we multiplied the robot power to α_r/α_h. The normalized power graphs are comparable, as shown in Fig. 6c.

4 Discussions & Future Outlook

In this work, we developed a hopper robot actuated from a hybrid electric-pneumatic actuator as an infrastructure for simultaneous adjustment of physical and virtual impedance. In this setup, the PAM pressure was adjusted to tune the physical impedance, and motors were controlled by a force feedback scheme, named FMCK, as a simplified bioinspired neural control for virtual impedance adjustment. The core concept of having physical impedance is supported

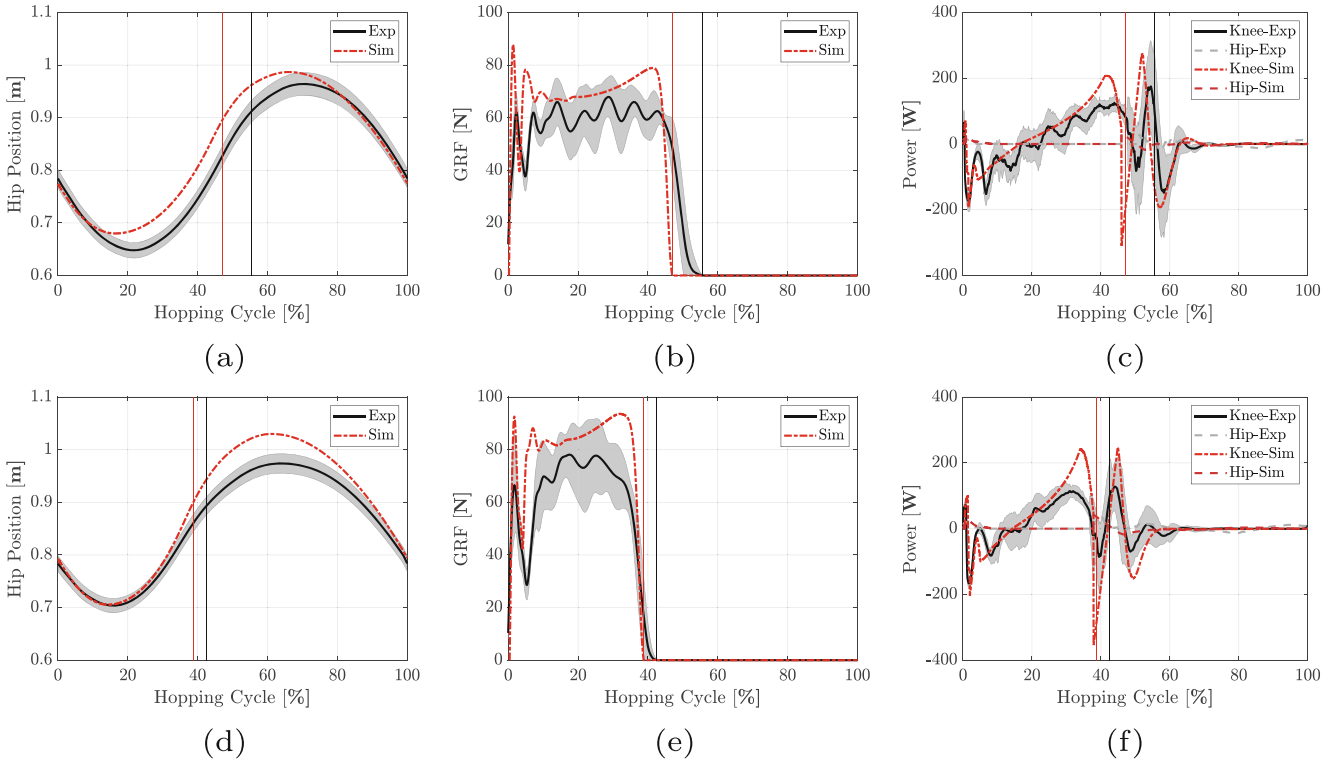

Fig. 5 Simulation and experimental results of EPA with and without PAM in a hopping cycle. The first row shows the results of EPA with the extensor PAM turned off completely, and the second row corresponds to the case where the PAM is inflated with constant pressure. (a,d) are the vertical displacement of hip in one period, (b,e) show the ground reaction force, and (c,f) display the knee and hip power, respectively. In all figures, simulation results are shown in dashed-dotted red lines, and the experimental results are plotted in solid black lines with their corresponding variance. Also, vertical red and black lines indicate the start of the flight phase for simulation and experimental data, respectively

by the human musculoskeletal system. Even with sufficiently high bandwidth, real-time reflection of a physical element cannot be exactly replicated by control. In [54], the dissimilarity of virtual and physical constraints in the developed dynamic behavior was analytically demonstrated. Improved efficiency, decreased dependency on sensors and motor functionality (e.g, noise effects) and control loop delay are the other advantages of using physical impedance [55] and [1].

4.1 Achievements of Blended Control with EPA

The aforementioned biological and mathematical pieces of evidence support the application of the PAMs as physical impedance besides the virtual impedance control in our EPA design. For repetitive movements, we suggested using the PAM as a tunable physical impedance while the electric motor continuously controls the total joint (or leg) impedance. Based on our simulation and experimental

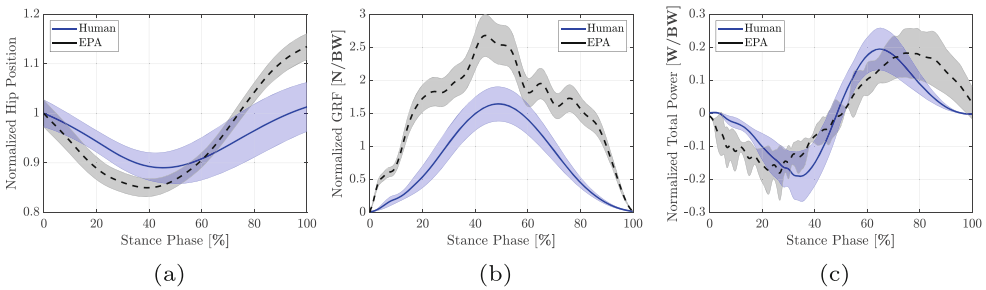

Fig. 6 Comparison of EPA-Hopper-II and human hopping experimental results in the stance phase. (a) hip position normalized by the hip height at landing, (b) GRF normalized by the body weight, (c) normalized total power consumed in the joints. In all figures, the solid and dashed graphs with their corresponding shaded areas depict the human and robot data (mean ± variance), respectively

studies, the achievements of this article, which will be discussed further in the following, can be summarized as 1) Successful implementation of a new bioinspired GRF-based control of virtual impedance, 2) Demonstrating the advantages of tuning the physical compliance (impedance), 3) Verifying the extendability of the proposed approach, and finally, 4) The ability to produce human-like hopping performance. In Section 4.2, we will also analyze the hybrid control of physical and virtual impedance control, supported by simulations, showing the great potential for significant improvement in efficiency and efficacy.

1) GRF-based virtual impedance control: Using virtual spring for generating bouncing behavior as in the SLIP (spring-loaded inverted pendulum) model [56] for hopping and running was already applied to robots [26] and [40]. Instead of emulating a fixed or switching virtual spring using a virtual model control (VMC) [39], [26], and [40], here the continuous GRF signal is employed for feedback control. As shown in Fig. 4, the normalized stiffness (C) and the rest angle (ϕ_{k0}) can be used to adjust hopping height. Clearly, ϕ_{k0} is more appropriate than C for tuning the hopping height. By selecting C between 0.2 and 0.3 m/rad, this adjustment can tune hopping height to any value below 25 cm. Generally speaking, increasing the rest angle of the virtual knee spring can reduce hopping height. Setting lower ϕ_0 means selecting more extended knee resting angles. Further, this value (besides the normalized stiffness) could also be utilized to decrease the consumed energy. For example, with $C = 0.3$ m/rad, changing ϕ_0 from 0° to 12° will reduce energy consumption by 16% while keeping the same hopping height. With this bioinspired control and a learning-based adaptation, we can first find the appropriate range for reaching a specific hopping height and then fine-tune the parameters to minimize energy consumption. This approach could be executed in a higher-level control (not investigated here).

In FMCK, the body load is the primary feedback signal for the virtual impedance control of the stance leg. From a broader perspective, legged locomotion can be described as a composition of three locomotor subfunctions (LSFs), namely stance (which characterizes the axial leg function), swing, and balance (posture control) [57]. The GRF-based control strategy, which is supported by the biological studies on healthy [58] and pathological gait [59] and [34] can provide further advantages in synchronizing different LSFs. In [60], a concerted control concept was introduced using the GRF signal as the leading signal from the conductor to harmonize the stance and balance LSFs as two key players of locomotion. Successful implementation of the GRF-based control to modulate ankle (FMCA) and hip (FMCH) joint impedance, respectively in a prosthetic foot [52] and an exoskeleton [61] could support the idea of concerted control at the joint level. In that respect, the FMCK could complement the FMCH [36] and FMCA [52] to generate a stable gait with coordinated joint movement led by the GRF as the conductor.

2) Adjustable physical impedance: Locomotion can be considered as a sequence of oscillatory motions [62]. It is known that each oscillatory system owns at least one natural frequency, in which it needs minimal control effort. To change the natural frequency, the mechanical property of the system should change. In a spring-mass system, either mass or stiffness of the spring can be used to tune the natural frequency. In our EPA-hopper design, the PAM pressure can be used to change the leg stiffness and, consequently, the natural frequency. If the desired frequency is close to the natural frequency, the effort from the electric motor (EM) can be minimized. The results of our simulations and experiments in Table 2 support the successful application of the PAM as a tunable physical impedance to adjust the natural frequency and, consequently, a more efficient hopping. Improving energy efficiency is not the only advantage of EPA design. Figure 5 demonstrates the filtering effect of the parallel PAM in the smoothened GRF and power graphs of the second-row pictures. The appropriate PAM pressure can also generate more human-like GRF patterns.

In our experiments (and simulations), PAMs are not used as the main energy resources, but as simple adjustable compliance. During performing a specific movement (hopping with a certain condition), no energy resources are required for the PAMs except the initial pressure adjustment, which is negligible in comparison to the total electrical energy for repetitive hops. PAM pressure adaptation could potentially increase energy efficiency by optimizing the absorption and recoiling the gravitational energy. In Section 4.2, we will show that an additional knee extensor PAM allows the motor to be off in the first half of the stance phase and then significantly reduce the required energy.

3) Extensibility of the proposed approach: Besides the bioinspired control approach, the combination of the EM and PAM in the EPA framework provides an extendable basis for versatile and efficient hopping. Inspired by human leg morphology, a three-segmented leg is well-fitted for a wide range of locomotion such as bouncing gaits [63]. By keeping the control architecture and extending the robot with the additional foot segment, we examined the extensibility and modularity of the EPA-based robot design and GRF-based control. Interestingly, without another energy source for the ankle, a passively compliant joint complemented the implemented control of the hip and knee joint and generated stable hopping. Although the elastic behavior of the ankle joint in human hopping was previously demonstrated [64], achieving stable hopping without changing any control parameter was not expected.

Table 2 Simulation (*Sim*) and Experiment (*Exp*) results of EPA obtained from implementing different control approaches concerning virtual and physical impedance

Controller \ Metric		P [MPa]	f [Hz]	h [cm]	E [J]	ρ
FMCK - No PAM	(*Sim*)	0	1.71	20.22	37.17	30.68
FMCK - No PAM	(*Exp*)	0	1.53	17.89	40.59	24.85
FMCK - Const. PAM	(*Sim*)	0.6	1.80	24.55	36.73	37.24
FMCK - Const. PAM	(*Exp*)	0.6	1.81	19.16	39.68	26.62

The FMCK control parameters for all cases are considered as $C = 0.07$ and $\phi_{k0} = 0$

This level of robustness against changing system dynamics might come from the FMCK control and the built-in physical compliance. In other words, the GRF feedback includes the required information about the system status, which can be complemented by the considered elastic behavior inducted by the physical impedance. Based on these findings, we envision extending the proposed design and control framework to generate robust and efficient forward hopping, bipedal hopping, and running. In doing so, taking insights from other locomotor systems that generate locomotion by leveraging from the passive dynamics and using interactions of internal impact force and external static friction can also be helpful [65, 66].

4) Mimicking human hopping: By approaching the human leg morphology in EPA-Hopper-II, the resulting behavior also approached human hopping. As shown in Fig. 6, the kinematic and kinetic patterns became more similar to those of humans than in the EPA-hopper-I with the 2-segmented leg. Despite the comparable hopping height, the robot performance is not as symmetric as human hopping. However, the comparable GRF magnitude and pattern, normalized to the body weight, supports the biologically inspired design and control of EPA-Hopper-II. Further, the consumed power required to reach a certain hopping height (relative to the leg length) is similar between humans and the robot. This result means that the efficiency of our EPA-based robot approaches the human hopping efficiency. Therefore, learning from human mechanics and control in the design and control of the hopper robot successfully provided comparable outcomes.

4.2 Harnessing the Potential of PAMs

So far, we have discussed virtual impedance control using the FMCK and constant PAM pressure for physical impedance control. To better analyze the coevolution of controlling these two impedance sources, we utilize the template & anchor concept [67]. Although the hybrid dynamics of locomotion complicates periodic motion stability analyses, the combination of mass and spring could provide template models to better support understanding of the motion [56] and [62]. To represent the hybrid dynamics of vertical hopping considering both stance and flight phase, two masses connected with spring were used as a template model [68] and [44]. Although this system is not a smooth oscillator, the addition of a periodic actuation force to the spring can compensate losses (e.g., impact) and generate a smooth system [68] and [62]. With this argumentation which was mathematically proved in [68], the combination of the EM and PAM could perfectly generate a smooth oscillatory hopping motion. To provide a realistic expectation of the EPA design potentials, we examined more advanced versions of the proposed blended control in another simulation study with the EPA-Hopper-I robot.

1) Hybrid state-based control of physical and virtual impedance adjustment: Inspired by the human [43] and the robot hopping (Figs. 5c and 5f), we modified the FMCK-based EPA control by switching off the motors in the downward movement. Thus, the knee extensor PAM instead of the knee motor provides the required opposing torque (to gravity) to decelerate the robot motion in the first half of the stance phase (deceleration phase).

Here, we carried out the simulations in two cases to investigate the performance of this control approach. In the first case, C1, we used two parallel extensor PAMs with the same fixed pressure while controlling the electric motors with the FMCK method only after reaching the maximum compression. The second PAM could compensate for the missing motor contribution in the first half of the stance phase.

In the second case, C2, we repeated the same approach but with the addition of a third extensor PAM coming to play simultaneously with the motor in the acceleration phase (second half of the stance phase). Therefore, the third PAM is activated at the maximum compression moment by injecting air pressure and is deactivated by depleting air pressure as the flight phase begins.

In order to simulate these cases, the controller parameters are chosen as $C = 0.032$ and $C = 0.012$ m/rad for C1 and C2 cases, respectively, while $\phi_{k0} = 0$ for both. The reason for lowering the controller gain in these simulations is for comparison purposes, as these values are chosen to generate comparable hopping height to scenario B (see Section 3.2).

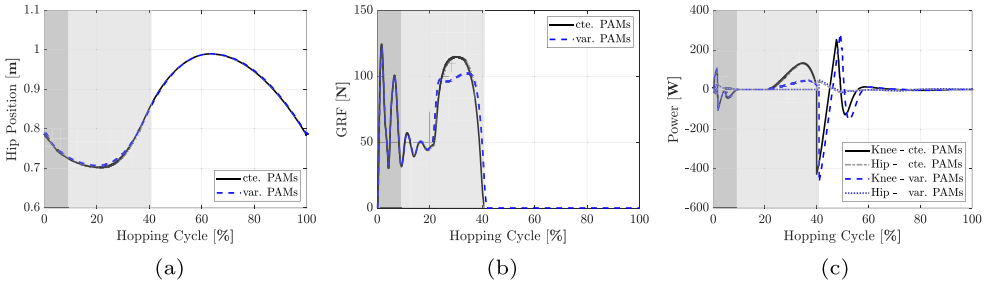

Fig. 7 Results obtained from simulating EPA with modified FMCK and constant/variable PAMs. Shaded dark gray and light gray areas in these figures depict the collision phase (wherein the transition PD controller is used) and the stance phase of hopping, respectively

The results are shown in Fig. 7. An insight into these figures reveals that both cases resulted in stable movements, with similar hopping heights; $h = 24.55$ cm. We expect less energy consumption by eliminating the knee joint's negative work in the deceleration phase (Fig. 7c). Calculation of the energy consumption for the first and second cases gives $E = 26.18$ J and $E = 23.58$ J, which shows a reduction of 28.7% and 35.8% in energy consumption compared to the scenario B presented in Section 3.2. Similarly, the efficacy for these cases increased to $\rho = 52.80$ and $\rho = 58.68$.

2) Higher performance with lower energy consumption: Utilizing two parallel PAMs with fixed pressure could significantly reduce the load on the knee motor by switching it off in the first half of the stance phase. Compared to the actuation with only EM, here EPA can increase the hopping height by 21% (to 24.55 cm) while decreasing about 30% of the consumed energy (compared to Table 2). Hence, this augmentation in EPA design yields a 71% increase in efficacy (ρ) of motion (compared to scenario A). The simple two-level PAM pressure adjustment during hopping in case C2 could generate an acceptable improvement (about 13%) in energy consumption (compared to C1). Further elaborate PAM control as adjustable physical compliance could also raise the benefits.

4.3 Outlook

Our hybrid actuator design is a key feature that provides access to investigate body intelligence [9] in terms of identifying the role of reflex control and mechanics. We demonstrated higher stability, energy efficiency, and performance using the blended control with the EPA design. Other motion control characteristics such as robustness against uncertainties or perturbations, and adaptation to different environmental or gait conditions are other topics to be tested with the EPA technology and the blended control. In [33], we demonstrated the role of parallel PAMs (in EPA-hopper-I) for increasing robustness against ground-level perturbations.

Compared to human motor control, the functionality of the PAM pressure, which could emulate the stimulation signal for muscle activation, was not fully perceived in our control implementation. Coordination between the virtual and physical impedance control can be improved by using feedback control for PAMs. One approach could be implementing a GRF-based pressure control similar to the FMCK. GRF could also synchronize the virtual and physical impedance control at one joint in such a condition. Thus, we need to compromise between control complexity and efficacy. Adjusting the PAM pressure during locomotion might improve efficacy (performance and efficiency), while it complicates control and increases sensitivity to measurement uncertainties and noises.

Developing a stable, performant, and efficient robot was not the only target of this study. With the bioinspired design and control, we also intended to generate human-like movements and understand the role of leg morphology and motor control in human gaits. The first step to approach human leg morphology was the addition of the foot to the 2-segmented leg. Surprisingly, the FMCK controller, which was designed for the 2-segmented leg, was also able to stabilize the robot with one extra degree of freedom thanks to the passive compliant ankle design. Furthermore, having a closer leg morphology to the human leg increased the behavioral similarity to human hopping. Still, few muscles were modeled by the EPA-Hopper-II, which can be extended by additional EPA actuators representing the other mono- and bi-articular muscles, as shown in Fig. 1. Our preliminary experiments (not shown) supported the important role of the gastrocnemius muscle in hopping. This result supports the idea of morphological computation, which can significantly simplify control. Therefore, EPA-based robots and blended control can be utilized as a practical tool for reverse engineering human locomotion control. The identified principles can be applied in the design and control of assistive devices [69].

Acknowledgements The authors would like to thank Guoping Zhao, Ferréol Gagey, Ayoob Davoodi, and Ryu Takahashi for providing experimental support in this study.

Author Contributions Omid Mohseni is the corresponding author of the article, contributed in the simulation modeling, carried out the robot experiments, implemented control approaches both in simulations and experiments, prepared the results, and contributed in data analysis and drafting the manuscript. Aida Mohammadi Nejad Rashty carried out the human hopping experiments, worked on acquisition, analysis, and interpretation of experimental human data,

and contributed in doing the robot experiments. Andre Seyfarth made substantial contributions to the conception of the work, contributed in interpretation of data, discussions, and commenting on and writing the article. Koh Hosoda also contributed in conception of the study, and revised it critically for important intellectual content. Maziar Ahmad Sharbafi was responsible for the conception of the work, designing and supervising both human and robot simulations/experiments, analysis and interpretation of data, and writing the manuscript. All authors gave final approval for participation.

Funding Open Access funding enabled and organized by Projekt DEAL. ThisThis work was supported by the German Research Foundation (Deutsche Forschungsgemeinschaft - DFG) funded EPA Project [grant number AH307/2-1] and [grant number SE1042/29-1], and EPA 2 Project [grant number AH307/4-1].

Declarations

Ethics approval The human hopping experimental study was approved by the Ethical Committee of the Technical University of Darmstadt.

Consent to participate All subjects voluntarily provided written informed consent to participate in the hopping experiments.

Consent for Publication All subjects gave consent to publish their data prior to submitting the manuscript to a journal.

Competing interests The authors have no conflicts of interest to declare that are relevant to the content of this article.

References

1. Pratt, G.A., Williamson, M.M.: Series elastic actuators. In: Proceedings 1995 IEEE/RSJ International Conference on Intelligent Robots and Systems. Human Robot Interaction and Cooperative Robots, vol. 1, pp. 399–406 (1995). IEEE
2. Seok, S., Wang, A., Chuah, M.Y., Otten, D., Lang, J., Kim, S.: Design principles for highly efficient quadrupeds and implementation on the mit cheetah robot. In: 2013 IEEE International Conference on Robotics and Automation, pp. 3307–3312 (2013). IEEE
3. Seyfarth, A., Blickhan, R., Van Leeuwen, J.: Optimum take-off techniques and muscle design for long jump. J. Exp. Biol. **203**(4), 741–750 (2000)
4. Hosoda, K., Rode, C., Siebert, T., Vanderborght, B., Weckx, M., Lefeber, D.: Actuation in Legged Locomotion. In: Bioinspired Legged Locomotion, pp. 563–622. Elsevier, Amsterdam (2017)
5. Nishikawa, K., Biewener, A.A., Aerts, P., Ahn, A.N., Chiel, H.J., Daley, M.A., Daniel, T.L., Full, R.J., Hale, M.E., Hedrick, T.L., Lappin, A.K., Nichols, T.R., Quinn, R.D., Satterlie, R.A., Szymik, B.: Neuromechanics: an integrative approach for understanding motor control. Integr. Comp. Biol. **47**(1), 16–54 (2007)
6. Liu, X., Rosendo, A., Ikemoto, S., Shimizu, M., Hosoda, K.: Robotic investigation on effect of stretch reflex and crossed inhibitory response on bipedal hopping. J R Soc Interface. **15**(140), 20180024 (2018)
7. Hobbelen, D., De Boer, T., Wisse, M.: System overview of bipedal robots flame and tulip: Tailor-made for limit cycle walking. In: 2008 IEEE/RSJ International Conference on Intelligent Robots and Systems, pp. 2486–2491 (2008). IEEE
8. Spröwitz, A., Tuleu, A., Vespignani, M., Ajallooeian, M., Badri, E., Ijspeert, A.J.: Towards dynamic trot gait locomotion: Design, control, and experiments with cheetah-cub, a compliant quadruped robot. Int J Rob Res **32**(8), 932–950 (2013)
9. Pfeifer, R., Lungarella, M., Iida, F.: Self-organization, embodiment, and biologically inspired robotics. Science **318**(5853), 1088–1093 (2007)
10. Ambrose, E., Ames, A.D.: Improved performance on moving-mass hopping robots with parallel elasticity. arXiv:1909.12930 (2019)
11. Iida, F.: Cheap design approach to adaptive behavior: Walking and sensing through body dynamics. In: International Symposium on Adaptive Motion of Animals and Machines, p. 15 (2005). Citeseer
12. Karssen, J.G.D., Wisse, M.: Running with improved disturbance rejection by using non-linear leg springs. Int J Rob. Res. **30**(13), 1585–1595 (2011)
13. Ahmadi, M., Buehler, M.: Controlled passive dynamic running experiments with the ARL-monopod II. IEEE Trans. Robot. **22**(5), 974–986 (2006)
14. Sharbafi, M.A., Rode, C., Kurowski, S., Scholz, D., Möckel, R., Radkhah, K., Zhao, G., Rashty, A.M., von Stryk, O., Seyfarth, A.: A new biarticular actuator design facilitates control of leg function in biobiped3. Bioinspir. Biomim. **11**(4), 046003 (2016)
15. Mettin, U., La Hera, P.X., Freidovich, L.B., Shiriaev, A.S.: Parallel elastic actuators as a control tool for preplanned trajectories of underactuated mechanical systems. Int J Rob. Res. **29**(9), 1186–1198 (2010)
16. Sharbafi, M.A., Yazdanpanah, M.J., Nili, M., Seyfarth, A.: Parallel compliance design for increasing robustness and efficiency in legged locomotion – proof of concept IEEE Transaction on Mechatronics 24(4) (2019)
17. Shahri, M.A., Mohseni, O., Bidgoly, H.J., Ahmadabadi, M.N.: Profile design of parallel rotary compliance for energy efficiency in cyclic tasks. IEEE/ASME Trans Mechatron. **25**(1), 142–151 (2019)
18. Mohseni, O., Shahri, M.A., Davoodi, A., Ahmadabadi, M.N.: Adaptation in a variable parallel elastic actuator for rotary mechanisms towards energy efficiency. Robot. Auton. Syst. **143**, 103815 (2021)
19. Ham, R.v., Sugar, T., Vanderborght, B., Hollander, K., Lefeber, D.: Compliant actuator designs. IEEE Robot. Autom. Mag. **3**(16), 81–94 (2009)
20. Nasiri, R., Zare, A., Mohseni, O., Yazdanpanah, M.J., Ahmadabadi, M.N.: Concurrent design of controller and passive elements for robots with impulsive actuation systems. Control. Eng. Pract. **86**, 166–174 (2019)
21. Yesilevskiy, Y., Xi, W., Remy, C.D.: A comparison of series and parallel elasticity in a monoped hopper. In: 2015 IEEE International Conference on Robotics and Automation (ICRA), pp. 1036–1041 (2015). IEEE
22. Karssen, J.G.D.: Robotic Bipedal Running: Increasing Disturbance Rejection. PhD thesis, Delft University of Technology (2013)

23. Beckerle, P., Verstraten, T., Mathijssen, G., Furnémont, R., Vanderborght, B., Lefeber, D.: Series and parallel elastic actuation: Influence of operating positions on design and control. IEEE ASME Trans. Mechatron. **22**(1), 521–529 (2016)
24. Verstraten, T., Beckerle, P., Furnémont, R., Mathijssen, G., Vanderborght, B., Lefeber, D.: Series and parallel elastic actuation:, Impact of natural dynamics on power and energy consumption. Mech. Mach. Theory **102**, 232–246 (2016)
25. Pratt, J., Krupp, B.: Design of a bipedal walking robot. Unmanned Syst. Technol X **6962**, 69621 (2008). International Society for Optics and Photonics
26. Sharbafi, M.A., Radkhah, K., von Stryk, O., Seyfarth, A.: Hopping control for the musculoskeletal bipedal robot: Biobiped. In: 2014 IEEE/RSJ International Conference on Intelligent Robots and Systems, pp. 4868–4875 (2014). IEEE
27. Vanderborght, B., Albu-schäffer, A., Bicchi, A., Burdet, E., Caldwell, D.G., Carloni, R., Catalano, M., Eiberger, O., Friedl, W., Ganesh, G., Garabini, M., Grebenstein, M., Grioli, G., Haddadin, S., Hoppner, H., Jafari, A., Laffranchi, M., Lefeber, D., Petit, F., Stramigioli, S., Tsagarakis, N., Damme, M.V., Ham, R.V., Visser, L.C., Wolf, S.: Variable impedance actuators:, A review. Rob. Auton. Syst. **61**(12), 1601–1614 (2013)
28. Ahmad Sharbafi, M., Shin, H., Zhao, G., Hosoda, K., Seyfarth, A.: Electric-pneumatic actuator: A new muscle for locomotion. In: Actuators, vol. 6, p. 30 (2017). Multidisciplinary Digital Publishing Institute
29. Mohseni, O., Gagey, F., Zhao, G., Seyfarth, A., Sharbafi, M.A.: How far are pneumatic artificial muscles from biological muscles? In: 2020 IEEE International Conference on Robotics and Automation (ICRA), pp. 1909–1915 (2020). IEEE
30. Klute, G.K., Czerniecki, J.M., Hannaford, B.: Mckibben artificial muscles: pneumatic actuators with biomechanical intelligence. In: 1999 IEEE/ASME International Conference on Advanced Intelligent Mechatronics (Cat. No. 99TH8399), pp. 221–226 (1999). IEEE
31. Daerden, F., Lefeber, D.: Pneumatic artificial muscles: actuators for robotics and automation. Eur. J Mech. Environ. Eng. **47**(1), 11–21 (2002)
32. Vanderborght, B., Verrelst, B., Van Ham, R., Van Damme, M., Lefeber, D., Duran, B.M.Y., Beyl, P.: Exploiting natural dynamics to reduce energy consumption by controlling the compliance of soft actuators. Int J Rob. Res. **25**(4), 343–358 (2006)
33. AhmadSharbafi, M., Yazdanpanah, M.J., Ahmadabadi, M.N., Seyfarth, A.: Parallel compliance design for increasing robustness and efficiency in legged locomotion-theoretical background and applications. IEEE ASME Trans. Mechatron. **25**(4), 1–12 (2020)
34. Dietz, V., Horstmann, G., Trippel, M., Gollhofer, A.: Human postural reflexes and gravity?an under water simulation. Neurosci. Lett. **106**(3), 350–355 (1989)
35. Duysens, J., Clarac, F., Cruse, H.: Load-regulating mechanisms in gait and posture: comparative aspects. Physiol. Rev. **80**(1), 83–133 (2000)
36. Sharbafi, M.A., Seyfarth, A.: Fmch: a new model for human-like postural control in walking. In: 2015 IEEE/RSJ International Conference on Intelligent Robots and Systems (IROS), pp. 5742–5747 (2015). IEEE
37. Sharbafi, M.A., Naseri, A., Seyfarth, A., Grimmer, M.: Neural Control in Prostheses and Exoskeletons. In: Powered Prostheses: Design, Control and Clinical Application. Elsevier, ??? (2020)
38. Galljamov, R., Ahmadi, A., Mohseni, O., Seyfarth, A., Beckerle, P., Sharbafi, M.A.: Adjustable compliance and force feedback as key elements for stable and efficient hopping. IEEE Robot. Autom. Lett **6**(4), 6797–6804 (2021)
39. Pratt, J., Dilworth, P., Pratt, G.: Virtual model control of a bipedal walking robot. In: Proceedings of International Conference on Robotics and Automation, vol. 1, pp. 193–198 (1997). IEEE
40. Oehlke, J., Beckerle, P., Seyfarth, A., Sharbafi, M.A.: Human-like hopping in machines. Biol. Cybern. **113**(3), 227–238 (2019)
41. Junius, K., Moltedo, M., Cherelle, P., Rodriguez-Guerrero, C., Vanderborght, B., Lefeber, D.: Biarticular elements as a contributor to energy efficiency: biomechanical review and application in bio-inspired robotics. Bioinspir. Biomim. **12**(6), 061001 (2017)
42. Kenneally, G., De, A., Koditschek, D.E.: Design principles for a family of direct-drive legged robots. IEEE Robot. Autom. Lett **1**(2), 900–907 (2016)
43. Rashty, A.M.N., Grimmer, M., Seyfarth, A.: Hopping frequency influences elastic energy reuse with joint series elastic actuators. J. Biomech. **110319**, 119 (2021)
44. Kalveram, K.T., Haeufle, D.F., Seyfarth, A., Grimmer, S.: Energy management that generates terrain following versus apex-preserving hopping in man and machine. Biol. Cybern. **106**(1), 1–13 (2012)
45. Oehlke, J., Sharbafi, M.A., Beckerle, P., Seyfarth, A.: Template-based hopping control of a bio-inspired segmented robotic leg. In: 2016 6th IEEE International Conference on Biomedical Robotics and Biomechatronics (BioRob), pp. 35–40 (2016). IEEE
46. Geyer, H., Seyfarth, A., Blickhan, R.: Positive force feedback in bouncing gaits? Proceedings of the Royal Society of London. Series B:, Biological Sciences **270**(1529), 2173–2183 (2003)
47. Haeufle, D., Grimmer, S., Seyfarth, A.: The role of intrinsic muscle properties for stable hopping—stability is achieved by the force–velocity relation. Bioinspir. Biomim. **5**(1), 016004 (2010)
48. Schumacher, C., Seyfarth, A.: Sensor-motor maps for describing linear reflex composition in hopping. Front. Comput. Neurosci. **11**, 108 (2017)
49. Zhao, G., Szymanski, F., Seyfarth, A.: Bio-inspired neuromuscular reflex based hopping controller for a segmented robotic leg. Bioinspir. Biomim. **15**(2), 026007 (2020)
50. Haeufle, D., Grimmer, S., Kalveram, K.T., Seyfarth, A.: Integration of intrinsic muscle properties, feed-forward and feedback signals for generating and stabilizing hopping. J R Soc. Interface. **9**(72), 1458–1469 (2012)
51. Davoodi, A., Mohseni, O., Seyfarth, A., Sharbafi, M.A.: From template to anchors: transfer of virtual pendulum posture control balance template to adaptive neuromuscular gait model increases walking stability. R. Soc. Open Sci. **6**(3), 181911 (2019)
52. Naseri, A., Grimmer, M., Seyfarth, A., Sharbafi, M.A.: Neuromechanical force-based control of a powered prosthetic foot. Wearable Technologies **1** (2020)
53. Delp, S.L., Anderson, F.C., Arnold, A.S., Loan, P., Habib, A., John, C.T., Guendelman, E., Thelen, D.G.: Opensim: open-source software to create and analyze dynamic simulations of movement. IEEE Trans. Biomed. Eng. **54**(11), 1940–1950 (2007)
54. Westervelt, E.R., Grizzle, J.W., Chevallereau, C., Choi, J.H., Morris, B.: Feedback Control of Dynamic Bipedal Robot Locomotion. Taylor & Francis, CRC Press, ??? (2007)
55. Braun, D.J., Chalvet, V., Chong, T.H., Apte, S.S., Hogan, N.: Variable stiffness spring actuators for low-energy-cost human augmentation. IEEE Trans. Robot. **35**(6), 1435–1449 (2019)
56. Blickhan, R.: The spring-mass model for running and hopping. J. Biomech. **22**(11-12), 1217–1227 (1989)
57. Sharbafi, M.A., Lee, D., Kiemel, T., Seyfarth, A.: Fundamental Subfunctions of Locomotion. In: Bioinspired Legged Locomotion, pp. 11–53 (2017). Elsevier, ???
58. Dietz, V., Leenders, K., Colombo, G.: Leg muscle activation during gait in parkinson's disease: influence of body unloading. Electroencephalography and Clinical Neurophysiology/Electromyography and Motor Control **105**(5), 400–405 (1997)
59. Dietz, V., Duysens, J.: Significance of load receptor input during locomotion: a review. Gait & posture **11**(2), 102–110 (2000)
60. Sarmadi, A., Schumacher, C., Seyfarth, A., Sharbafi, M.A.: Concerted control of stance and balance locomotor subfunctions—leg

force as a conductor. IEEE Trans. Med. Robot. Bionics **1**(1), 49–57 (2019)
61. Zhao, G., Henning, V., Seyfarth, A.: Neuromuscular Reflex Based Hopping Control for a Two-Segmented Robotic Leg. In: 9 International Symposium on Adaptive Motion of Animals and Machines (AMAM 2019) (2019)
62. Revzen, S., Kvalheim, M.: Locomotion as an Oscillator. In: Bioinspired Legged Locomotion, pp. 97–110 (2017). Elsevier
63. Seyfarth, A., Günther, M., Blickhan, R.: Stable operation of an elastic three-segment leg. Biol. Cybern. **84**(5), 365–382 (2001)
64. Farley, C.T., Morgenroth, D.C.: Leg stiffness primarily depends on ankle stiffness during human hopping. J. Biomech. **32**(3), 267–273 (1999). https://doi.org/10.1016/S0021-9290(98)00170-5
65. Liu, P., Yu, H., Cang, S.: Optimized adaptive tracking control for an underactuated vibro-driven capsule system. Nonlinear Dynamics **94**(3), 1803–1817 (2018)
66. Liu, P., Neumann, G., Fu, Q., Pearson, S., Yu, H.: Energy-efficient design and control of a vibro-driven robot. In: 2018 IEEE/RSJ International Conference on Intelligent Robots and Systems (IROS), pp. 1464–1469 (2018). IEEE
67. Full, R.J., Koditschek, D.E.: Templates and anchors: neuromechanical hypotheses of legged locomotion on land. J. Exp. Biol. **202**(23), 3325–3332 (1999)
68. Burden, S.A., Revzen, S., Sastry, S.S.: Model reduction near periodic orbits of hybrid dynamical systems. IEEE Trans. Autom. Control **60**(10), 2626–2639 (2015)
69. Firouzi, V., Davoodi, A., Bahrami, F., Sharbafi, M.A.: From a biological template model to gait assistance with an exosuit. Bioinspir. Biomim. **16**(6), 066024 (2021)

Omid Mohseni received the B.Sc. degree in Electrical Engineering from Azad University, Karaj Branch (KIAU), Iran, in 2014, and the M.Sc. in Control Engineering from the University of Tehran (UT), Iran, in 2017. He then continued as a research assistant in the Lauflabor Locomotion Laboratory at the Institute of Sports Science of the Technische Universität Darmstadt, under the supervision of Prof. Andre Seyfarth. Currently, he is a Ph.D. candidate at the Department of Electrical Engineering and Information Technology, TU Darmstadt, under the co-supervision of Prof. Andre Seyfarth and Prof. Mario Kupnik. His research interests focus on biomechanics, bio-inspired legged locomotion, compliant actuation, and learning.

Aida Mohammadi Nejad Rashty received her B.Sc. and M.Sc. degree in Electrical-Control Engineering from the K.N. Toosi University of Technology (KNTU) in Tehran, Iran, in 2004 and 2007, respectively. She is a Ph.D. candidate in the Lauflabor Locomotion Lab at the Institute of Sports Science and the center of cognitive science of the Technical University of Darmstadt, under the supervision of Prof. Andre Seyfarth. She is involved in national (DFG, Germany) and international (EU) research projects since 2013. Her research interests are on biomechanics, human locomotion analysis and modeling, and bio-inspired legged locomotion.

Andre Seyfarth received the Vordiplom degree in physics, the Diploma degree (including B.Sc. and M.Sc.) in physics and biomechanics, and the Ph.D. degree in biomechanics from Friedrich-Schiller Universität at Jena, Jena, Germany, in 1991, 1995, and 2000, respectively. He is currently a Professor of sports biomechanics with the Department of Human Sciences, TU Darmstadt and the Head of the Lauflabor Locomotion Lab. After his studies in physics, he went as a DFG "Emmy Noether" fellow to the MIT LegLab (Prof. Herr, USA) and the ParaLab at the university hospital Balgrist, Zurich (Prof. Dietz, Switzerland). His research interests include sport science, human and animal biomechanics, and legged robots.

Koh Hosoda received the Ph.D. degree in mechanical engineering from Kyoto University, Kyoto, Japan, in 1993. He was an Assistant Professor in the Department of Mechanical Engineering from 1993 to 1997, and an Associate Professor in the Graduate School of Engineering from 1997 to 2010, at Osaka University. He was a Guest Professor in the Artificial Intelligence Laboratory, University of Zurich, from April 1998 to March 1999. He was a group leader of JST Asada ERATO Project from 2005 to 2010. From 2010 to 2014, he was a Professor in the Graduate School of Information Science and Technology, Osaka University. Since 2014, he has been a Professor in the Graduate School of Engineering Science, Osaka University.

Maziar Ahmad Sharbafi received the B.Sc. degree from the Sharif University of Technology, Tehran, Iran, in 2003, and the M.Sc. and Ph.D. degrees from the University of Tehran, Tehran, Iran, in 2006 and 2013, respectively, both in control engineering. He received a second Ph.D. degree in biomechanics from TU Darmstadt, Darmstadt, Germany, in 2017. He is currently an Assistant Professor with the Electrical and Computer Engineering Department, University of Tehran, Tehran, Iran and a Guest Researcher with the Lauflabor Locomotion Laboratory, TU Darmstadt. His research interests include bioinspired locomotion control based on conceptual and analytic approaches, postural stability, and the application of dynamical systems, and nonlinear control to legged robots and exoskeletons.